Light nuclei production in relativistic Au+nucleus collisions

M. J. Bennett,[1] J. K. Pope,[1] D. Beavis,[2] J. B. Carroll,[3] J. Chiba,[4] A. Chikanian,[1] H. J. Crawford,[5] M. Cronqvist,[5] Y. Dardenne,[5] R. Debbe,[2] T. Doke,[6] J. Engelage,[5] L. Greiner,[5] R. S. Hayano,[7] T. J. Hallman,[3] H. H. Heckman,[8] T. Kashiwagi,[6] J. Kikuchi,[6] B. S. Kumar,[1] C. Kuo,[5] P. J. Lindstrom,[8] J. W. Mitchell,[9] S. Nagamiya,[10] J. L. Nagle,[1] P. Stankus,[10] K. H. Tanaka,[4] R. C. Welsh,[11] and W. Zhan[10]

(The E878 Collaboration)

[1]*Yale University, A.W. Wright Nuclear Structure Laboratory, New Haven, Connecticut 06511*
[2]*Brookhaven National Laboratory, Upton, New York 11973*
[3]*University of California at Los Angeles, Los Angeles, California 90095*
[4]*KEK, Tsukuba, Japan*
[5]*University of California Space Sciences Laboratory, Berkeley, California 94720*
[6]*Waseda University, Science and Engineering Research Institute, Waseda, Japan*
[7]*University of Tokyo, Tokyo, Japan*
[8]*E. O. Lawrence Berkeley National Laboratory, Berkeley, California 94720*
[9]*USRA/Goddard Space Flight Center, Greenbelt, Maryland 20771*
[10]*Columbia University, Nevis Laboratory, Irvington, New York 10533*
[11]*Johns Hopkins University, Baltimore, Maryland 21218*

(Received 26 March 1998)

We have measured the yields of protons and $A=2-4$ nuclei in collisions between 10.8A GeV/c Au beams and targets of Al, Cu, and Au. The data, which cover a broad rapidity range at low transverse momenta, were measured as a function of collision centrality using a focusing beam line spectrometer and a high-rate centrality detector. We investigate the dependence of coalescence parameters on event geometry. The data are compared with the predictions of an RQMD+coalescence model. [S0556-2813(98)00808-5]

PACS number(s): 25.75.+Dw

I. INTRODUCTION

Several experimental groups are trying to create unusual states of nuclear matter using high-energy nucleus-nucleus collisions. From previous experimental efforts at the Bevalac, at the AGS, and at the SPS [1–3], a plausible qualitative picture for the behavior of hadronic matter in these interactions has been developed. The collision of two nuclei creates a volume of highly compressed nuclear matter, and the resulting pressure gradients then drive an outward expansion. Among the more promising tools for the study of the expansion of the system and its volume at freeze-out is the measurement of production spectra of protons and light nuclei.

The currently accepted picture of the formation of nuclei near central rapidities in relativistic nucleus-nucleus interactions is that of *coalescence* [4–10]. Nuclei are believed to be formed in final-state interactions between nucleons, when other strong interactions have effectively ceased (i.e., at hadronic *freeze-out*) and nucleons happen to be close together in six-dimensional phase space. For a given combination of A nucleons, the probability that they will coalesce to form a nucleus of mass number A depends on the amount of overlap between the nucleon wave functions in both momentum and position space. Since both momentum and position variables play a role, the production rates of light nuclei relative to those of free nucleons are sensitive to the size of the nucleon source at freeze-out [8,11,12,18]. Correlations between momenta of nucleons with small relative spatial separations—as might result from collective flow or incomplete stopping—can enhance production in certain regions of phase space. The measurements and analysis of the Si+Pb data of experiment E814 [12, 18] showed that the collision volume expanded significantly before freeze-out. In this paper, we are able to extend their work to heavier colliding systems (Au+Au) and to heavier coalesced nuclei (^{3}He and ^{4}He). We emphasize that, because heavier isotopes are composed of more nucleons, their coalescence probabilities become more sensitive to any physical effect which changes the momentum and spatial configurations of nucleons. Thus, one might imagine a case in which a small effect in proton production goes unnoticed in the deuteron spectra, but would be evident in the $A=3$ or $A=4$ species. As will be seen, our

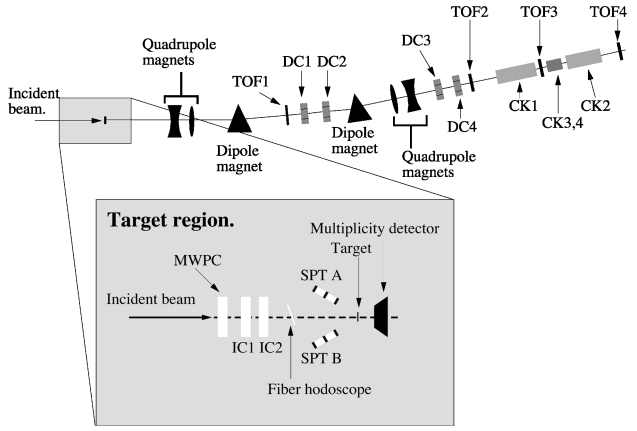

FIG. 1. Schematic diagram of the E878 beam line spectrometer. The inset is a detail of the target and the detectors surrounding it. The beam is incident from the left-hand side of the figure.

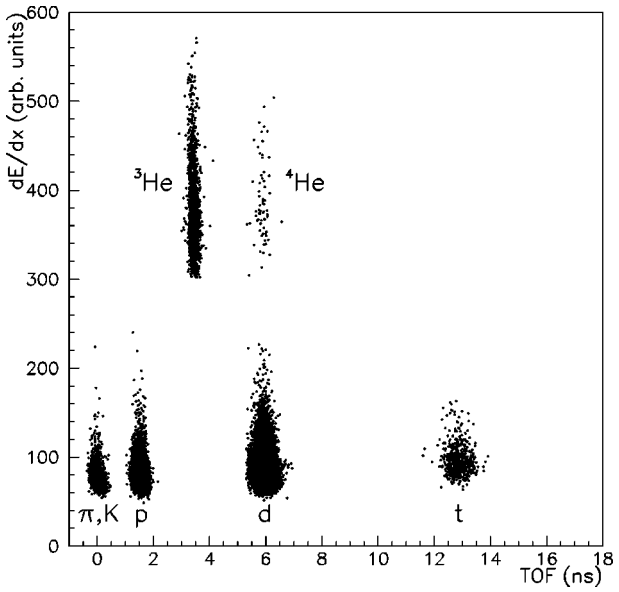

FIG. 2. Identification of positive particles at a rigidity $p/Z = 5.10$ GeV/c. The plot shows energy loss versus the time of flight measured in scintillation counters. Clearly identifiable in these plots are π and K, p, d, t, ^{3}He, and ^{4}He. Note that this plot represents the sum of various trigger conditions, which have been downscaled by different amounts. Thus, the relative populations of each species in the plot are not indicative of actual particle ratios.

data set provides good statistics for nuclei with $A=3$, and makes a reasonable measurement for $A=4$ particles as well.

We present here our measurements of the production rates of protons (p), deuterons (d), tritons (t), ^{3}He, and ^{4}He in collisions of Au beams on Au, Cu, and Al targets. These data were taken in the autumn of 1993 at the Brookhaven National Laboratory, using 10.8A GeV/c Au beams from the Alternating Gradient Synchrotron.

II. APPARATUS

Figure 1 is a schematic view of the E878 apparatus [14], which comprises a beam line focusing spectrometer. Charged secondary particles which are emitted within a roughly rectangular aperture of solid angle $\Delta\Omega \sim 350$ μsr centered on the beam axis, and with a rigidity (ratio of momentum to electric charge) within $\pm\sim 2\%$ of the chosen tuned rigidity, are transported through the spectrometer. Two sets of dipole magnets provide a double selection on rigidity; quadrupole magnets bring the secondaries to focal points at the centers of the trigger time-of-flight counters TOF 1 and TOF 3. Two additional arrays of counters, TOF 2 and TOF 4, provide a second measurement of velocity. The measured times of flight provide most of the particle identification capability; gas Čk 1 and Čk 2) and Aerogel (Čk 3 and Čk 4) threshhold Cerenkov detectors provide supplementary information for very fast secondaries. Four drift chambers DC 1–4, each containing six drift planes, are used in tracking and primarily provide background rejection for trajectories not pointing back to the target.

TABLE I. Proton invariant multiplicities in minimum-bias Au+Al, Au+Cu, and Au+Au reactions. Uncertainties are 30% systematic.

Rigidity (GeV/c)	Invariant multiplicity $E\ d^3N/dp^3$ (GeV^{-2} c^3)		
	Au+Al	Au+Cu	Au+Au
2.55	3.1±0.9	5.3 ± 1.6	7.1 ± 2.1
3.87	4.4±1.3	5.8 ± 1.7	7.7 ± 2.3
5.10	7.2±2.2	9.5 ± 2.9	9.8 ± 3.0
6.00	9.9±3.0	11.4 ± 3.4	12.9 ± 3.9

The data set presented in this work comes from four separate rigidity settings of the E878 spectrometer: +2.55, +3.87, +5.1, and +6.0 GeV/c (the positive sign indicating that accepted particles have $Z>0$). Data were collected using Al, Cu, and Au targets; the Au target had a thickness such that 22% of the Au beam underwent inelastic interactions, while the Al and Cu targets interacted with 27% of the Au beam.

For normalization purposes, several detectors are placed upstream of the target to monitor the incident beam. A multiwire proportional chamber (MWPC) and a fiber Cerenkov hodoscope located near the target measure the beam profile. Ion chambers (IC 1 and IC 2) located upstream of the target measure the integrated flux of the primary beam. The ion chambers are complemented by single-particle telescopes (SPT's) which count secondary particles emitted at backward angles to measure the fraction of the beam actually striking our target on a run-by-run basis. An array of quartz Cerenkov counters [13] samples the multiplicity of secondary particles produced in interactions and allows us to determine the centrality of a given interaction.

Triggers are generated by a particle in the spectrometer via a coincidence between the timing signals from two of the

TABLE II. Proton invariant multiplicities as functions of event centrality in Au+Al, Au+Cu, and Au+Au reactions. Uncertainties are 30% systematic.

	Invariant multiplicity $E\ d^3N/dp^3$ (GeV^{-2} c^3)				
Rigidity (GeV/c)	Au+Al Central 0–10 %	Au+Cu Central 0–10 %	Central 0–10 %	Au+Au Midcentral 10–30 %	Peripheral 30–100 %
2.55	3.5±1.0	8.9±2.7	16.5±4.9	9.7±2.9	5.0±1.5
3.87	4.0±1.2	9.4±2.8	17.5±5.2	11.2±3.4	5.4±1.6
5.10	6.2±1.9	14.3±4.3	19.5±5.8	13.1±3.9	7.5±2.3
6.00	7.5±2.3	16.0±4.8	21.9±6.6	16.2±4.9	10.6±3.2

TABLE III. Deuteron invariant multiplicities in minimum-bias Au+Al, Au+Cu, and Au+Au reactions. Uncertainties are 30% systematic.

Rigidity (GeV/c)	Invariant multiplicity $E\ d^3N/dp^3$ (GeV^{-2} c^3)		
	Au+Al	Au+Cu	Au+Au
2.55	0.055±0.017	0.132±0.040	0.258±0.077
3.87	0.061±0.018	0.106±0.032	0.187±0.056
5.10	0.083±0.025	0.133±0.040	0.188±0.056
6.00	0.101±0.030	0.147±0.044	0.214±0.064

time-of-flight detectors (TOF 1 and TOF 3). The simplest implementation of this trigger scheme, referred to as LOOSE, utilized a coincidence window which selected flight times between 0 ns (relative to $\beta=1$) and 80 ns, which would correspond to $\beta=0.53$. In addition, other trigger types were utilized; the most important with respect to light nuclei was a timing trigger (TIME), which required a delayed coincidence between TOF 1 and 3. The delay was chosen to select only those particles with M/Z greater than that of the proton, so that the delay was different for each tuned rigidity. Combined with downscaling of LOOSE triggers, the use of TIME allowed the collection of high statistics data for nuclei heavier than protons.

Because triggers are based on the detection of a particle in the spectrometer, the E878 cross sections are inherently minimum bias. While a multiplicity detector [13] was part of the apparatus, it was not utilized at the trigger level; rather, the multiplicity information allowed characterization of the geometry of an event after the detected produced particle had been identified. In this manner, events were separated into various bins of centrality: for Al and Cu targets, particles from the 10% most central events could be identified, while for Au targets, the data sample was separated into three centrality bins. These bins were ''peripheral,'' corresponding to the 70% most peripheral interactions; ''mid-central,'' corresponding to those events between 30% and 10% most central; and ''central,'' corresponding to the 10% most central interactions.

For the data set presented here, the operating configuration of the multiplicity detector was not the same as that described in [13]. Effectively, the difference was manifested in a lower efficiency of the multiplicity detector for the positive rigidity running. The calibration of the positive configuration was accomplished by correlating the multiplicity spectra of pions and kaons from data taken at the same rigidity in both the low- and high-efficiency configurations. This was cross-checked by calculating the efficiency for each of the 28 individual detectors in the multiplicity detector array (these ranged between 65% and 90%), and reperforming the Monte Carlo simulation of the detector response, as described in detail in [13]. The results of these two approaches agreed with each other quite well, and led to the definition of the bins described above.

III. ANALYSIS

Particle identification is accomplished primarily via $T13$, the time of flight between TOF 1 and TOF 3, which were separated by ~27.5 m, augmented by a charge measurement in each of TOF 1 and TOF 3. For all of the rigidity settings considered here, individual nuclear species were well separated in $T13$-charge space, as can be seen for the +5.1 GeV/c setting in Figure 2 (this statement does not apply to pion-kaon separation, which can be achieved via Čerenkov information). Quality cuts have been applied which effectively remove all of the background. These cuts include agreement of velocity determined by $T13$ with that determined from the time of flight between TOF 2 and TOF 4, hits in all four TOF detectors, charge agreement between all four TOF hits, and a trajectory which points back to the target. Of these, all have very high efficiency ($\gtrsim$98%), except the requirement of TOF agreement. Here, the efficiency of the cut is 85%, which is consistent with expectations based on the tightness of the cut and the greater relative variation in actual path length between TOF 2 and TOF 4 (as compared to TOF 1 and TOF 3) for various trajectories within the beam envelope.

The total number of observed particles included some background from nontarget-related sources. This background level was determined by measuring the target-out detection rate using an empty target holder instead of a real target; this target-out rate was then converted to a number of background particles by scaling with the total beam flux and live time for a given run. Nontarget-related events have a different multiplicity distribution than that for true beam-target interactions; therefore, it was necessary to make a target-out correction individually for each of the defined centrality bins, based on the observed multiplicity distributions from the target-out running. The total background for minimum-bias events was roughly 10% of the total signal, consistent with our expectations based on the amount of material upstream

TABLE IV. Deuteron invariant multiplicities as functions of event centrality in Au+Al, Au+Cu, and Au+Au reactions. Uncertainties are 30% systematic.

Rigidity (GeV/c)	Invariant multiplicity $E\ d^3N/dp^3$ (GeV^{-2} c^3)				
	Au+Al Central 0–10 %	Au+Cu Central 0–10 %	Au+Au Central 0–10 %	Au+Au Midcentral 10–30 %	Au+Au Peripheral 30–100 %
2.55	0.065±0.019	0.216±0.065	0.540±0.162	0.361±0.108	0.189±0.057
3.87	0.066±0.020	0.192±0.058	0.454±0.136	0.283±0.085	0.122±0.037
5.10	0.088±0.026	0.232±0.070	0.471±0.141	0.278±0.083	0.121±0.036
6.00	0.094±0.028	0.250±0.075	0.507±0.152	0.317±0.095	0.143±0.043

TABLE V. Triton invariant multiplicities in minimum-bias Au+Al, Au+Cu, and Au+Au reactions. Uncertainties are 30% systematic.

Rigidity (GeV/c)	$10^4\times$invariant multiplicity $E\,d^3N/dp^3$ (GeV^{-2} c^3)		
	Au+Al	Au+Cu	Au+Au
3.87	7.8±2.3	24.0±7.1	59.2±17.8
5.10	9.4±2.8	21.9±6.6	38.6±11.6
6.00	10.8±3.2	19.1±5.7	36.4±10.9

of the target; when the rate was separated into centrality bins, the background was highest in the Au+Au peripheral bin, with an average of 15%, while the background for the Au+Au most-central bin was negligible.

Particles heavier than protons satisfied conditions for both LOOSE and TIME triggers; cross sections presented here were calculated using the TIME trigger condition, since the higher statistics allowed separation of the particles into the various centrality bins. However, some inefficiency in the TIME trigger is expected because of the close proximity of the various particle species in $T13$ space as compared to jitter in the trigger timing. Efficiency of the TIME trigger for deuterons and ^{3}He was estimated by comparing the numbers of minimum-bias (i.e., with no condition on centrality) particles of each species from TIME and from LOOSE trigger conditions. The efficiency for deuterons was ~85% for all rigidities, while that for ^{3}He ranged from 66% at the lowest rigidity to 60% at the highest rigidity. Low statistics precluded a separate determination of the TIME efficiency for ^{4}He and tritons; for ^{4}He, it was taken to be the same as that for deuterons, while a value of 90% was estimated for tritons based on their large $T13$ separation from protons. Since all events had to satisfy at least the LOOSE trigger condition in order to be recorded, it was not possible to make a direct determination of the LOOSE trigger efficiency in the usual manner. We have estimated the efficiency to be 95%, based on the simple trigger logic and scaler values for the count rates of the phototubes involved.

The total flux of the beam into our target region was integrated using two ionization chambers IC 1 and IC 2. The fraction of the beam actually striking our target was monitored using two single-particle telescopes SPT 1 and SPT 2; for all of the data considered here, the fraction of beam on target was ~100%. Performance and calibration of the beam monitoring detectors has been described in detail elsewhere [14]. The acceptance of the spectrometer was determined separately for each of the rigidity settings by comparing phase space distributions from actual data to Monte Carlo calculations [14]. Since the data necessarily include effects of multiple Coulomb scattering of particles as they traverse the beam line, a ''correction'' for this behavior is implicit in the calculated acceptance. For the data considered here, acceptances ($\Delta\Omega\Delta p/p$) ranged between 1110 and 1380 μsr %.

In addition, it was necessary to apply several correction factors to the observed cross sections, taking into account the live time fraction of the data acquisition system (DAQ), loss of beam flux in our target, and the loss of produced particles through inelastic interactions as they traverse the beam line. The live time of the data acquisition was determined by scaling various quantities gated by a $\overline{\text{BUSY}}$ signal from the DAQ computer indicating it was able to accept data, and comparing these to the same quantities from an ungated scaler. Live times for this data set ranged between 70% and 90%. In order to have high event rates, fairly thick targets were used; as the beam traverses the target, beam particles undergo interactions such that the downstream portion of the target effectively ''sees'' a lower beam flux. The magnitude of this effect can be calculated analytically, which resulted in a ''thick-target'' correction of 15% for Al and Cu targets and 12% for the Au target. The loss of particles via inelastic interactions with material in the beam line was estimated via Monte Carlo simulation [14]; the survival probability ranged between 80% for protons and 60% for ^{4}He, and was roughly independent of rigidity.

Invariant multiplicities for p, d, t, ^{3}He, and ^{4}He from minimum-bias Au+Al, Cu, and Au interactions are tabulated below. The quantity that E878 measures directly is the invariant cross section; however, in order to facilitate comparison to other experiments, values have been given in terms of invariant multiplicity. These have been determined by dividing the measured cross section by the total inelastic interaction cross section for the given beam-target system. The determination of these values is described in detail elsewhere [14]; the values are 6850 mb for Au+Au interactions, 4700 mb for Au+Cu, and 3750 mb for Au+Al. In addition, invariant multiplicities are also tabulated for various centrality bins for each of the beam-target systems, as defined in Sec. II. In this case, the measured cross section was divided by the cross section for the centrality condition applied; e.g., cross sections for 10% central Au+Au interactions were divided by 685 mb.

IV. RESULTS AND DISCUSSION

Tables I–X list the invariant multiplicities measured at four rigidity settings for p, d, t, ^{3}He, and ^{4}He. These mea-

TABLE VI. Triton invariant multiplicities as functions of event centrality in Au+Al, Au+Cu, and Au+Au reactions. Uncertainties are 30% systematic.

	$10^4\times$invariant multiplicity $E\,d^3N/dp^3$ (GeV^{-2} c^3)				
Rigidity (GeV/c)	Au+Al Central 0–10 %	Au+Cu Central 0–10 %	Au+Au Central 0–10 %	Au+Au Midcentral 10–30 %	Au+Au Peripheral 30–100 %
3.87	10.2±3.1	50.3±15.1	124.9±37.5	90.3±27.1	41.0±12.3
5.10	10.0±3.0	36.6±11.0	98.0±29.4	55.6±16.7	25.2± 7.6
6.00	9.5±2.9	42.0±12.6	86.4±25.9	55.6±16.7	23.8± 7.2

TABLE VII. ^{3}He invariant multiplicities in minimum-bias Au+Al, Au+Cu, and Au+Au reactions. Uncertainties are 30% systematic.

Rigidity (GeV/c)	$10^4\times$invariant multiplicity $E\ d^3N/dp^3$ (GeV^{-2} c^3)		
	Au+Al	Au+Cu	Au+Au
2.55	6.7±2.0	15.5±4.6	29.0±8.7
3.87	10.3±3.1	16.6±5.0	28.5±8.5
5.10	20.3±6.1	26.9±8.1	35.9±10.8
6.00	20.2±6.1	20.9±6.3	33.9±10.2

TABLE IX. ^{4}He invariant multiplicities in minimum-bias Au+Al, Au+Cu, and Au+Au reactions. Two uncertainty terms are shown: the first is statistical, and the second is 30% systematic.

Rigidity (GeV/c)	$10^6\times$invariant multiplicity $E\ d^3N/dp^3$ (GeV^{-2} c^3)		
	Au+Al	Au+Cu	Au+Au
2.55	11±4±3	41±9±12	71±25±21
3.87	22±4±7	30±6±9	40±7±12
5.10	51±8±15	49±13±15	93±11±28
6.00	79±8±24	85±10±26	168±13±50

surements are, in general, at different rapidities for the different particle species. The systematic uncertainties are quoted to be 30%, which is dominated by uncertainties in our determination of the beam flux and the acceptance of the spectrometer at each of the rigidity settings.

Figure 3 shows the invariant multiplicities for p, d, t, ^{3}He, and ^{4}He, plotted for minimum-bias Au+Al collisions as functions of rapidity. Also shown in the figure are data from experiment E814 for the Si+Pb system [12,18], which have been reflected about $y=1.72$ (the nucleon-nucleon center-of-mass rapidity at the Si beam energy of 14.6A GeV/c) to reverse the kinematics (the reverse kinematics Si+Pb system is very similar to Au+Al). The E814 data were measured at a slightly higher energy, and so the rapidities for the E814 data were scaled by 3.14/3.44 to match beam rapidities. The invariant multiplicities measured in our experiment agree well with those measured by E814, within systematic errors.

Figure 4 shows invariant multiplicity data for the same particle species measured in minimum bias Au+Cu collisions. Figure 5 shows similar data for the minimum-bias Au+Au system. In the cases of all the targets, the triton yields are higher than the ^{3}He yields, consistent with a neutron to proton ratio in excess of 1 in all of the colliding systems. In Fig. 5, we also show data measured by experiment E886 [19]. Although there is no direct rapidity overlap between the data of the two experiments, the trends of the measured cross sections indicate good agreement between E878 and E886. The yields of complex fragments in the E886 data increase significantly at low rapidity, perhaps reflecting the presence of light nucleus yields from fragmentation and/or the fact that the physical dimensions at freeze-out of the source of particles emitted in the the targetlike rapidities may be smaller than at midrapidity.

Figures 6, 7, and 8 show the yields of protons and light nuclei plotted as functions of rapidity for central Au+Al, Au+Cu, and Au+Au collisions. Near midrapidity, the yields in central collisions are higher than those in minimum-bias collisions. Also, the yields in the heavier systems are higher, over the full rapidity range of the measurement, than the yields in the lighter systems. For protons from central Au+Au collisions, although the distribution is flatter than that from minimum bias Au+Au events, there still remains a minimum in the spectrum at midrapidity. However, it is important to recall that E878 measures cross sections in a narrow p_T range around $p_T=0$, and that the presence of hydrodynamic flow can push particles away from low transverse momenta. Thus, expansion can lead to a dip at midrapidity in the invariant multiplicity distribution at low p_T, even while the dN/dy distributions, which are integrated over all transverse momenta, would be peaked at midrapidity, as has been observed by other experiments [20].

It should be noted that the primary motivation for the E878 experiment was to perform a high-statistics study of rare processes in heavy ion collisions, so that all components of the experimental apparatus were required to operate at high interaction rates. For the multiplicity detector, this requirement necessitated a relatively low number of channels. While the detector worked well, the low segmentation made the detector susceptible to statistical fluctuations in the phase space distribution of the secondary multiplicity. Thus, the various defined centrality bins have some contamination from events with less (or more) central geometries, as was detailed in [13]. The contamination was exacerbated somewhat (as compared to [13]) for the data shown here, due to the operating configuration of the multiplicity detector for the positive rigidity running (see Sec. II). For all comparisons to theoretical models, e.g. RQMD, we have been careful

TABLE VIII. ^{3}He invariant multiplicities as functions of event centrality in Au+Al, Au+Cu, and Au+Au reactions. Uncertainties are 30% systematic.

	$10^4\times$invariant multiplicity $E\ d^3N/dp^3$ (GeV^{-2} c^3)				
Rigidity (GeV/c)	Au+Al Central 0–10 %	Au+Cu Central 0–10 %	Au+Au Central 0–10 %	Au+Au Midcentral 10–30 %	Au+Au Peripheral 30–100 %
2.55	9.0±2.7	27.4± 8.2	74.3±22.3	45.7±13.7	17.8±5.4
3.87	10.8±3.2	31.7± 9.5	67.2±20.2	47.5±14.2	17.5±5.3
5.10	24.1±7.2	52.4±15.7	87.7±26.3	54.8±16.5	23.1±6.9
6.00	21.6±6.5	34.4±10.3	74.0±22.2	49.5±14.8	23.7±7.1

TABLE X. ^{4}He invariant multiplicities as functions of event centrality in Au+Al, Au+Cu, and Au+Au reactions. Two uncertainty terms are shown: the first is statistical, and the second is 30% systematic. Note that the point at a rigidity of 3.87 for central Au+Au collisions represents the detection of only a single particle in that bin.

	$10^4\times$invariant multiplicity $E\ d^3N/dp^3$ (GeV^{-2} c^3)				
	Au+Al	Au+Cu		Au+Au	
Rigidity (GeV/c)	Central 0–10 %	Central 0–10 %	Central 0–10 %	Midcentral 10–30 %	Peripheral 30–100 %
2.55	16±16±5	61±43±18	135±77±40	43±30±13	70±18±21
3.87	45±22±14	90±40±27	19±19±6	86±29±26	29±7±9
5.10	49±28±15	47±47±14	151±50±45	48±20±14	98±13±29
6.00	83±31±25	174±52±52	172±47±52	110±26±33	185±16±55

to match the E878 centrality conditions; the typical difference in yields from the E878-defined centrality conditions, as compared to an ''ideal'' centrality measurement (i.e., a hard cut in impact parameter), is on the order of 20–30 % for π, K, and protons in the RQMD model. (Note that this difference is not from some error in normalization, etc., but rather from the fact that the physics of the collision changes with the range of geometries sampled.) However, light nuclei yields are potentially much more sensitive to the centrality conditions, since their magnitude is, to first order, proportional to the proton yields raised to the Ath power. While it is possible to match centrality conditions when comparing to theoretical models, one needs to be very careful when comparing results between various experiments, especially those for light nuclei, since the conditions of the centrality cuts are necessarily different.

The formation of light nuclei near central rapidity in a nucleus-nucleus collision requires the constituent nucleons to be close together in phase space in order to be able to coalesce. Thus, the observed yields of light nuclei are sensitive to the detailed dynamical evolution of the system. The relative probability for the formation of a nuclear cluster is quantified in the B_A parameter, which is defined as the proportionality constant between the yield of a nucleus of mass number A and the Ath power of the proton yield:

$$E_A\frac{d^3N_A}{dp_A^3}=B_A\left(E_p\frac{d^3N_p}{dp_p^3}\right)^A, \tag{1}$$

where $p_A=Ap_p$. Our data set allows us to determine these ratios without fitting to the particle distributions, since we have proton, deuteron, ^{3}He, and ^{4}He measurements at $p_T\approx 0$ and $y_{\rm lab}=1.7$, just above y_{NN}.

Figure 9 shows the quantity B_A for various targets and event geometries in Au+A reactions. The data points correspond to events in different centrality bins, which are plotted against the mean number of participating nucleons for that bin (as determined by Monte Carlo simulation [14]). In our data set, B_2 decreases by a factor of 2 from the most-peripheral to the most-central bin, while B_3 decreases by a factor of 10 and B_4 by a factor of 100. However, it should be noted that, while the most-central and midcentral bins represent reasonably exclusive cuts on event geometry, the most-

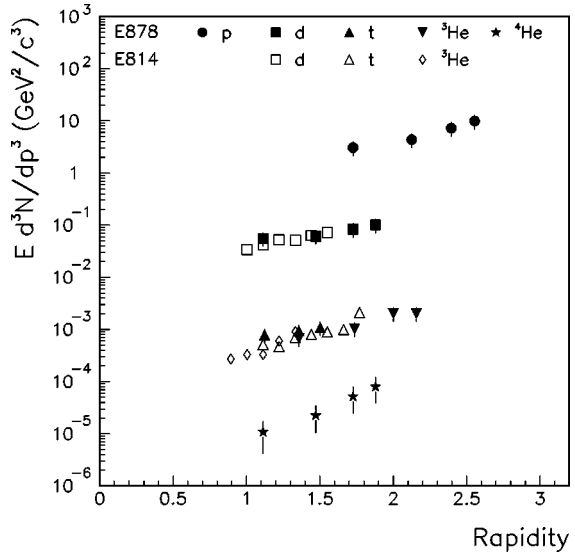

FIG. 3. Au+Al minimum-bias rapidity distributions at $p_T\approx 0$ for p, d, t, ^{3}He, and ^{4}He. Uncertainties are dominated by a 30% systematic error for all species except ^{4}He, which includes non-negligible statistical uncertainties added in quadrature with a 30% systematic uncertainty. Open symbols are data from minimum-bias E814 Si+Pb collisions, reflected about $y_{NN}=1.72$.

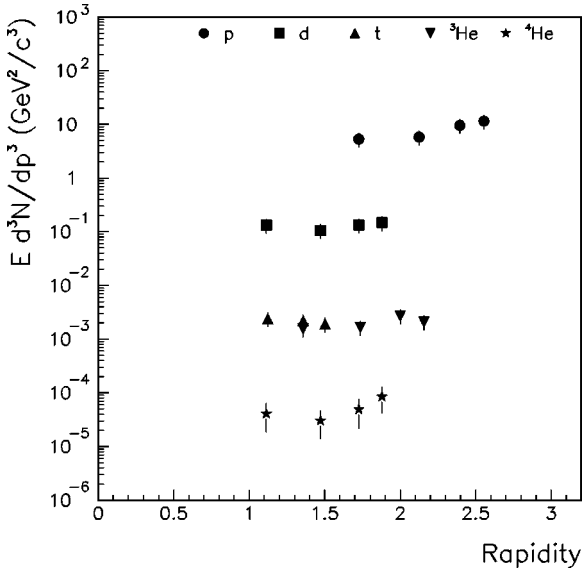

FIG. 4. Au+Cu minimum-bias rapidity distributions at $p_T\approx 0$ for p, d, t, ^{3}He, and ^{4}He. Uncertainties are dominated by a 30% systematic error for all species except ^{4}He, which includes non-negligible statistical uncertainties added in quadrature with a 30% systematic uncertainty.

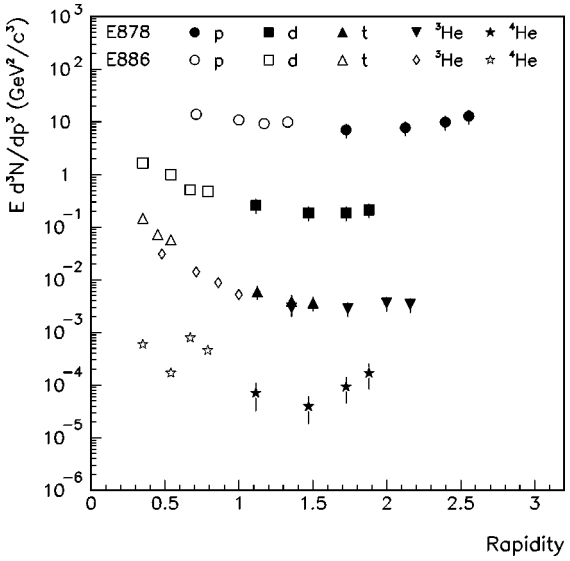

FIG. 5. Au+Au minimum-bias rapidity distributions at $p_T \approx 0$ for p, d, t, ^{3}He, and ^{4}He. Uncertainties are dominated by a 30% systematic error for all species except ^{4}He, which includes non-negligible statistical uncertainties added in quadrature with a 30% systematic uncertainty. The open symbols are the measurements of experiment E886 showing statistical and systematic uncertainties added in quadrature.

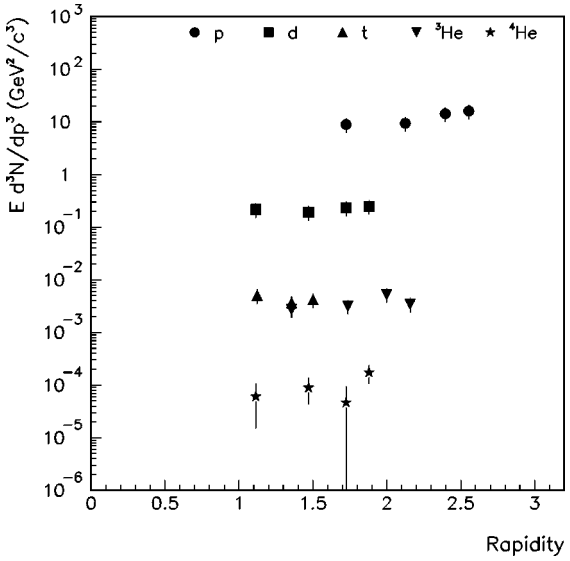

FIG. 7. Au+Cu central (10% highest multiplicity events) rapidity distributions at $p_T \approx 0$ for p, d, t, ^{3}He, and ^{4}He. Uncertainties are dominated by a 30% systematic error for all species except ^{4}He, which includes non-negligible statistical uncertainties added in quadrature with a 30% systematic uncertainty.

peripheral bin for Au+Au represents the 70% lowest-multiplicity events and thus averages over a large range in collision geometries. Data from the three targets are qualitatively consistent with one another.

In a thermal model, a change in the value of the B_A parameter can be related to a change in the volume of the source that is creating the composite particles [15]. If the size of the source increases, the average relative separation between nucleons also increases, so that the likelihood of two nucleons being close enough in position space to form a nuclear cluster, as quantified by B_A, is decreased. Several approaches have been developed to calculate a source radius based on B_A parameters, e.g., in thermal or density matrix models [16,17].

However, a similarity in B_A parameters for different interacting systems should not be taken to necessarily imply that the actual source sizes for the two systems are the same. As an example, if one were to apply one of the models mentioned above to calculate a source size based on our B_A parameters from central Au+Al interactions, the result would be considerably larger than an Al nucleus; this increase in size is understood to be the result of the hydrody-

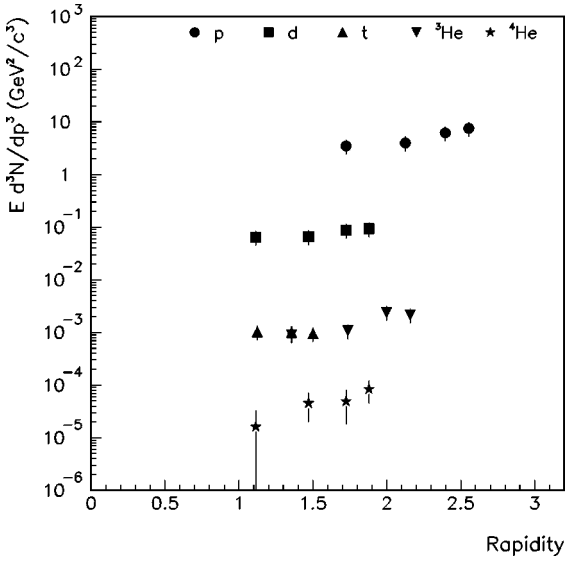

FIG. 6. Au+Al central (10% highest multiplicity events) rapidity distributions at $p_T \approx 0$ for p, d, t, ^{3}He, and ^{4}He. Uncertainties are dominated by a 30% systematic error for all species except ^{4}He, which includes non-negligible statistical uncertainties added in quadrature with a 30% systematic uncertainty.

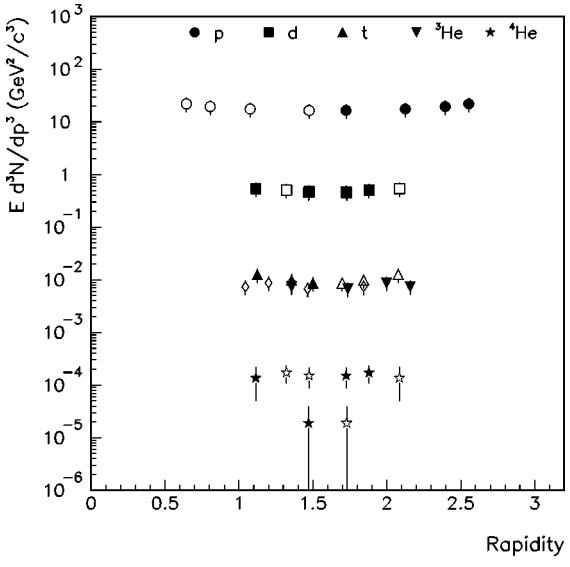

FIG. 8. Au+Au central (10% highest multiplicity events) rapidity distributions at $p_T \approx 0$ for p, d, t, ^{3}He, and ^{4}He. Uncertainties are dominated by a 30% systematic error for all species except ^{4}He, which includes non-negligible statistical uncertainties added in quadrature with a 30% systematic uncertainty.

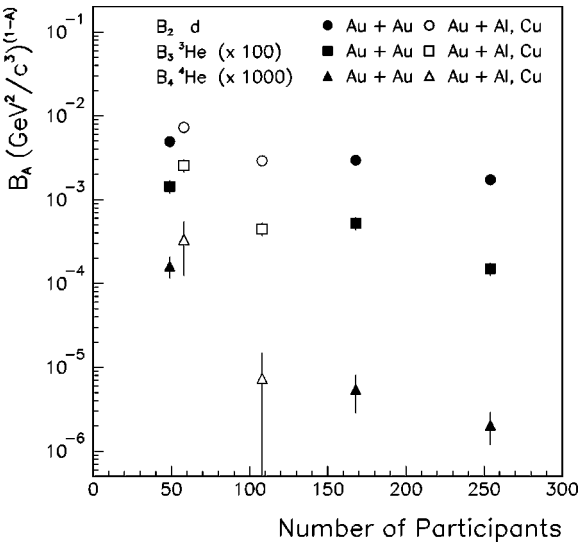

FIG. 9. Dependence of the B_A parameter on the number of participants in Au+Al, Au+Cu, and Au+Au reactions. For the Au+Au data, we show points for each of our three centrality bins; for the lighter targets, only the data from the ''most-central'' bin is shown.

namic expansion of the system. In addition to increasing the source size, and thus reducing B_A, the coherent nature of the hydrodynamic expansion also increases the likelihood of nucleons which are close to each other in position space to be close to each other in momentum space as well, which would increase B_A. Thus, a similarity between B_A values for two colliding systems may indicate a counterbalancing of increased hydrodynamic flow with increased source size. Interestingly, since the decrease we observe in B_A as a function of the number of participants (Fig. 9) is markedly steeper as the size of the coalesced cluster increases, it seems plausible that the A dependence of this parameter could be used to disentangle these competing effects. However, a meaningful effort at such a study should include particle production integrated over all phase space, which would require data from other experiments in addition to the E878 data shown here.

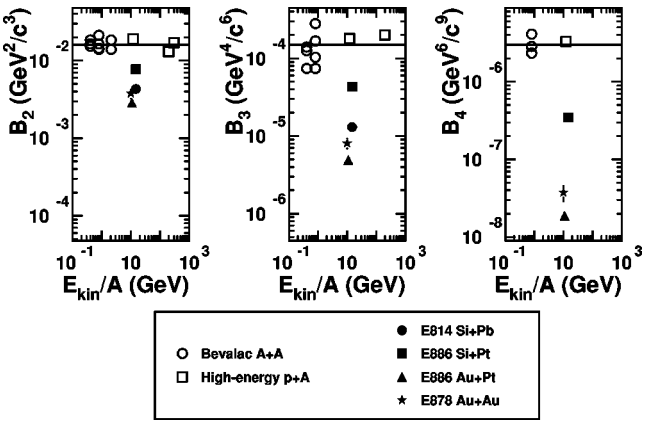

FIG. 10. Systematics of the B_A parameter as a function of projectile kinetic energy per nucleon measured for various minimum-bias nucleus-nucleus experiments. The horizontal lines are drawn to represent the trends of the $p+A$ and lower-energy data. The E814 data shown here are from [12,18], and the E886 data are from [19]; references for the non-AGS data are given in the text.

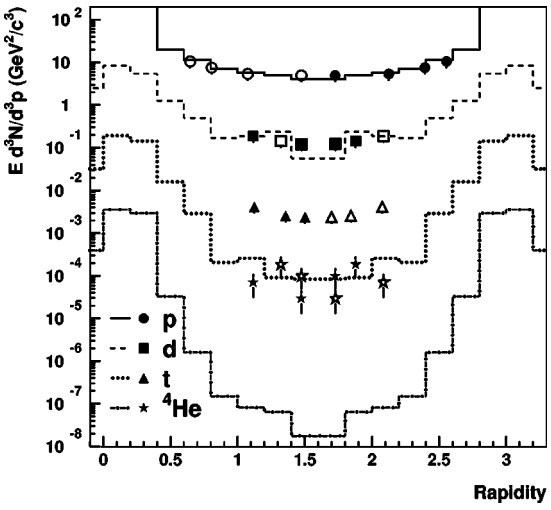

FIG. 11. The invariant multiplicities for p, d, t, and ^{4}He plotted as a function of rapidity for peripheral Au+Au collisions. The histograms are the predictions of the RQMD (version 2.2) [24] + coalescence model [7].

Figure 10 shows the quantities B_2, B_3, and B_4 as a function of projectile kinetic energy per nucleon. The open symbols represent minimum-bias values measured in many experiments, from nucleus-nucleus interactions at the Bevalac [21] at the lowest energies on the scale, to proton-nucleus collisions at KEK [19], the CERN SPS [22], and the Fermilab Tevatron [23] at the highest energies. In all of these measurements, the B_A parameters lie along the horizontal line shown in this figure, representing a constant mean value for the various data. In previous analyses of light nucleus production from nucleus-nucleus reactions at the AGS and at the CERN SPS [9], it was observed that the B_A values fell well below this line; a few representative data points for minimum bias $A+A$ collisions at the AGS are shown in Fig. 10. This effect was interpreted as an increase of the size of the source of nucleons at freeze-out. E878 data points for minimum-bias Au+Au collisions, also shown in Fig. 10, are

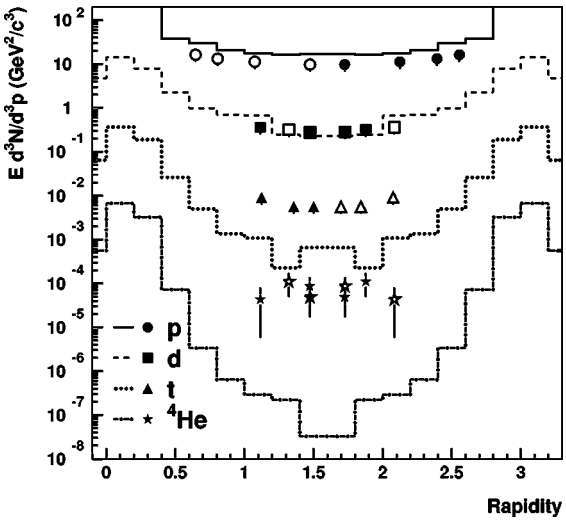

FIG. 12. The invariant multiplicities for p, d, t, and ^{4}He plotted as a function of rapidity for midcentral Au+Au collisions. The histograms are the predictions of the RQMD (version 2.2) [24] + coalescence model [7].

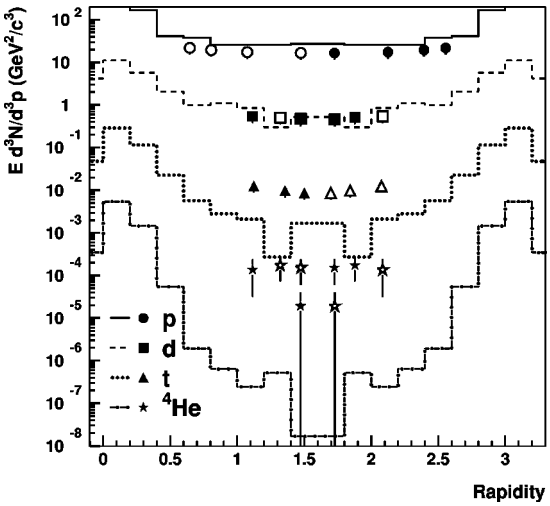

FIG. 13. The invariant multiplicities for p, d, t, and ^{4}He plotted as a function of rapidity for central Au+Au collisions. The histograms are the predictions of the RQMD (version 2.2) [24] + Coalescence model [7].

well below the average values. The trend of these points, in comparison to the lower-energy nucleus-nucleus data, is that of a rapid decrease in B_A (reflecting a systematic increase in the volume of the nuclear source) with beam energy. We can interpret this effect in the same framework used to explain the drop in B_A with the number of participants. Our data therefore show qualitative evidence for system expansion.

Between the systematic dependence of B_A on centrality and collision energy, we find support for our simple picture of an expanding system. Since there are the competing effects of increased source size (which decreases B_A) and collective flow (which increases B_A), simple models cannot be used to extract quantitative information about the dimensions and shapes of the collision volumes at freeze-out. One needs to resort to use of cascade models followed by coalescence.

Theoretical predictions for light nuclei yields were generated by performing a coalescence calculation (using the approach of [7]) on the output of RQMD version 2.2 [24], run in cascade mode. A comparison of E878 protons, deuterons, tritons, and ^{4}He to the resulting predictions is shown for Au+Au peripheral (Fig. 11), midcentral (Fig. 12), and central (Fig. 13) collisions. For this comparison, care has been taken to correctly match the centrality conditions imposed upon the model to those of the measurement. In the case of peripheral collisions, RQMD matches the proton and deuteron spectra reasonably well, but substantially underpredicts for tritons and ^{4}He. For midcentral and central collisions, RQMD roughly matches the shape of the E878 proton distribution, but overpredicts the magnitude by a factor of $\sim$2. As in the peripheral collisions, both tritons and ^{4}He from E878 lie well above the predicted values. Given the disagreement with the proton distributions and the direct dependence of larger composites on the proton distribution, it is probably not wise to try to read too much into the details of the disagreement of RQMD+coalescence with the E878 d, t, and ^{4}He. However, since the magnitude of the discrepancy is so large (e.g., several orders of magnitude for ^{4}He), it would be hard to ascribe the entire difference to a mismatch with the proton rapidity distribution. Other possible sources of disagreement with the data would be the coalescence prescription for nuclei with $A \geqslant 3$ and the detailed phase space output of nucleons from RQMD.

In two recent papers, Mattiello *et al.* have elucidated the importance of collective potentials in affecting the spectra of deuterons [6] and light nuclei [7]. They use an approach which adds baryonic mean field interactions to RQMD version 1.07, which is then followed by a coalescence calculation similar to that used for the comparisons above. For central Au+Au collisions, the yield of protons at $p_T/A \leqslant 0.5$ GeV/c and at midrapidity is decreased by $\sim$20% with the addition of potentials. The decrease in observed yield gets stronger with increasing A, so that the predicted yield of ^{4}He in the same kinematic regime is reduced by more than 50%. Unfortunately, since these predictions were produced with an ''ideal'' centrality cut (see discussion above) and light nuclei yields are very sensitive to centrality, a direct comparison to E878 data would be misleading. A reduction in protons at midrapidity, as [7] suggests mean fields would bring about, would lead to a better agreement between RQMD and E878. On the other hand, the trend with increasing A given in [7] would imply that the addition of potentials would lead to an even greater discrepancy with the E878 deuterons, tritons, and ^{4}He. However, the p_T range in that prediction is considerably larger than that of E878; any conclusion about the importance of potentials would require a more precise matching of the model prediction to the experimental conditions.

V. SUMMARY AND CONCLUSIONS

We have measured the spectra of p, d, t, ^{3}He, and ^{4}He in collisions of Au beams with targets of Al, Cu, and Au. We have presented invariant multiplicities for all of the systems in minimum bias and central collisions. Our data are in agreement with other measurements in regions where there is kinematic overlap. We discuss the variation of the coalescence parameter B_A with system, centrality, and collision energy. Our spectra show qualitative evidence for large freeze-out volumes and collective expansion. The predictions of the RQMD version 2.2 model [24], run in cascade mode, reproduce the shape of our measured proton spectra, but overpredict the magnitude of the proton yield for midcentral and central Au+Au collisions. The addition of a coalescence calculation to RQMD leads to predictions which are considerably lower than our data for tritons and ^{4}He, which suggests problems with either the coalescence prescription or the detailed phase space output from RQMD. However, since the proton spectra are the backbone of the coalescence calculation and RQMD does not match our protons, it would be premature to draw any detailed conclusions based on the magnitude of the discrepancy with the E878 light nuclei. We anticipate the availability of complementary data from experiments E864 [25], E866 [20] and E877 [26]. The combined data sets and improved calculations will allow for a better understanding of the collision environment and of composite particle production.

ACKNOWLEDGMENTS

We thank the Brookhaven AGS and Tandem staffs for providing the beam. We also thank R. Mattiello and H. Sorge for their help in obtaining and running the RQMD and coalescence codes. This work was supported in part by Grants Nos. DE-FG02-91ER-40609, DE-FG03-88ER-40424, and DE-FG03-90ER-40571 with the U.S. Department of Energy.

[1] *Quark Matter '96*, edited by P. Braun-Munzinger, H. J. Specht, R. Stock, and H. Stöcker [Nucl. Phys. **A610** (1996)].
[2] *Quark Matter '95*, edited by A. M. Poskanzer, J. W. Harris, and L. S. Schroeder [Nucl. Phys. **A590** (1995)].
[3] *Quark Matter '93*, edited by E. Stenlund, H.-Å. Gustafsson, A. Oskarsson, and I. Otterlund [Nucl. Phys. **A566** (1994)].
[4] S. T. Butler and C. A. Pearson, Phys. Rev. Lett. **7**, 69 (1961); Phys. Rev. **129**, 836 (1963).
[5] A. Baltz *et al.*, Phys. Lett. B **325**, 7 (1994).
[6] R. Mattiello *et al.*, Phys. Rev. Lett. **74**, 2180 (1995).
[7] R. Mattiello *et al.*, Phys. Rev. C **55**, 1443 (1997).
[8] J. L. Nagle *et al.*, Phys. Rev. Lett. **73**, 1219 (1994).
[9] J. L. Nagle, B. S. Kumar, D. Kusnezov, H. Sorge, and R. Mattiello, Phys. Rev. C **53**, 367 (1996).
[10] D. E. Kahana *et al.*, Phys. Rev. C **54**, 338 (1996).
[11] S. Mrowczynski, Phys. Lett. B **248**, 459 (1990).
[12] J. Barrette, *et al.*, Phys. Rev. C **50**, 1077 (1994).
[13] E878 Collaboration, D. Beavis *et al.*, Nucl. Instrum. Methods Phys. Res. A **357**, 283 (1995).
[14] M. J. Bennett, Ph.D. thesis, Yale University, 1995.
[15] A. Z. Mekjian, Phys. Rev. Lett. **38**, 640 (1977); Phys. Rev. C **17**, 1051 (1978); S. Das Gupta and A. Z. Mekjian, Phys. Rep. **72**, 131 (1981).
[16] R. Bond, P. J. Johansen, S. E. Koonin, and S. Garpman, Phys. Lett. **71B**, 43 (1977).
[17] H. Sato and K. Yazaki, Phys. Lett. **98B**, 153 (1981).
[18] J. Germani, Ph.D. thesis, Yale University, 1994.
[19] E886 Collaboration, N. Saito *et al.*, Phys. Rev. C **49**, 3211 (1994).
[20] F. Videbaek for the E802 Collaboration, in *Quark Matter '95*, edited by A. M. Poskanzer, J. W. Harris, and L. S. Schroeder [Nucl. Phys. **A590** 249c (1995)].
[21] S. Nagamiya *et al.*, Phys. Rev. C **24**, 971 (1981); R. L. Auble, *ibid.* **28**, 1552 (1983).
[22] W. Bozzoli, Nucl. Phys. **B116**, 317 (1978).
[23] J. W. Cronin *et al.*, Phys. Rev. D **11**, 3105 (1975).
[24] H. Sorge, Phys. Rev. C **52**, 3291 (1995); H. Sorge, R. Mattiello, H. Stocker, and W. Greiner, Phys. Lett. B **271**, 37 (1991).
[25] J. K. Pope, Ph.D. thesis, Yale University, 1997.
[26] E877 Collaboration, S. C. Johnson *et al.*, in ''Heavy Ion Physics at the AGS,'' edited by C. A. Pruneau *et al.*, Wayne State University Report No. WSU-NP-96-16, Detroit, MI, 1996, p. 112.